High resolution imaging in cross-section of a metal-oxide-semiconductor field-effect-transistor using super-higher-order nonlinear dielectric microscopy

N Chinone, K Yamasue, K Honda and Y Cho

Research Institute of Electrical Communication, Tohoku University, 2-1-1, Katahira, Aoba-ku, Sendai 980-8577, Japan

chinone@riec.tohoku.ac.jp

Abstract. Scanning nonlinear dielectric microscopy (SNDM) can evaluate carrier or charge distribution in semiconductor devices. High sensitivity to capacitance variation enables SNDM to measure the super-high-order (higher than 3rd) derivative of local capacitance-voltage (C-V) characteristics directly under the tip ($\mathrm{d}^nC/\mathrm{d}V^n, n=3,4,\cdots$). We demonstrate improvement of carrier density resolution by measurement of $\mathrm{d}^nC/\mathrm{d}V^n, n=1,2,3,4$ (super-higher-order method) in the cross-sectional observation of metal-oxide-semiconductor field-effect-transistor.

1. Introduction

The requirement for small, high-speed, and high-function large scale integrated circuits (LSIs) and large scale memories has been promoting miniaturization of transistors in these devices [1]. Widely known as Moore's law, the number of electric devices in LSIs has been exponentially increased with exponential decrease of device scale [1]. According to prediction by International Technology Roadmap of Semiconductors, this trend will continue and the required gate length of transistor will go down to less than 10 nm within the next 10 years [2]. Commercially, flash memories containing transistors whose scale is less than 20 nm are already available [3]. In research, a transistor with 3 nm of gate length has been achieved [4]. However, highly advanced miniaturization enhances the difficulty of suppressing the fluctuation of device properties arising from random spatial dopant distribution [5]. In addition, the trend of low voltage operation devices [2] enhances the influence of the fluctuation. Therefore, a technique for analysing small variation of carrier density with high spatial resolution is indispensable for developing present and future device performance.

Scanning probe microscopies (SPMs) are promising technique for measuring nanometer-scale devices with high spatial resolution. As a purpose of carrier concentration analysis in semiconductor devices, for example, scanning spreading resistance microscopy (SSRM) [6], scanning capacitance microscopy (SCM) [7], and scanning nonlinear dielectric microscopy (SNDM) [8] have been used. Among these SPMs, SNDM can analyse carrier or charge distribution thorough local capacitance-voltage (C-V) measurement. In previous studies, carrier distribution in metal-oxide-semiconductor field-effect-transistor (MOSFET) and stored charge distribution in flash memory were clearly visualized [9–11]. For SNDM, detectable minimum capacitance variation is typically 10^{-22} F [12]. This high sensitivity enables SNDM to acquire not only the 1st order response of capacitance to

Content from this work may be used under the terms of the Creative Commons Attribution 3.0 licence. Any further distribution of this work must maintain attribution to the author(s) and the title of the work, journal citation and DOI.
Published under licence by IOP Publishing Ltd

external voltage ($\mathrm{d}C_\mathrm{s}/\mathrm{d}V$), but also the *n*-th order response ($\mathrm{d}^n C_\mathrm{s}/\mathrm{d}V^n$), where $n \geq 2$ [13, 14]. We here call the term $\mathrm{d}^2 C_\mathrm{s}/\mathrm{d}V^2$ higher-order term and the term $\mathrm{d}^n C_\mathrm{s}/\mathrm{d}V^n$ ($n \geq 3$) super-higher-order term. The higher-order and super-higher-order terms are more sensitive to capacitance variation compared to $\mathrm{d}C_\mathrm{s}/\mathrm{d}V$ term. Measurement of up to super-higher-order terms (super-higher-order method) [14] enables us to detect small variations of C-V characteristics caused by small carrier density variation.

Previously, we reported that super-higher-order imaging could reveal more detailed structure of a MOSFET compared to 1st and 2nd order images [14]. In this paper, we focus on carrier density in the dopant area of a MOSFET and demonstrate that the super-higher-order method is able to clarify slight spatial variation of carrier density.

2. Principle of SNDM

SNDM measures capacitance variation under the sharp conductive tip through frequency modulation and demodulation [8]. Figure 1 shows a schematic diagram of SNDM which is based on contact-mode atomic force microscopy (AFM). The probe of SNDM consists of a metal-coated cantilever tip and an active LC oscillator, whose oscillating frequency *f* is determined by tip-sample capacitance C_s, static capacitance C_0 (including built-in and stray capacitance), and built-in inductance *L*. When the C_s has nonlinear dependence on the external voltage *V* applied between sample and grounded tip, the *f* is modulated by *V*. When $V = V_\mathrm{DC} + V_\mathrm{p}\cos\omega_\mathrm{p} t$, the variation of C_s is approximately described as follows [14].

$$\Delta C_\mathrm{s} \approx \left.\frac{\mathrm{d}C_\mathrm{s}}{\mathrm{d}V}\right|_{V_\mathrm{DC}} V_\mathrm{p}\cos\omega_\mathrm{p} t + \frac{1}{4}\left.\frac{\mathrm{d}^2 C_\mathrm{s}}{\mathrm{d}V^2}\right|_{V_\mathrm{DC}} {V_\mathrm{p}}^2 \cos 2\omega_\mathrm{p} t + \frac{1}{24}\left.\frac{\mathrm{d}^3 C_\mathrm{s}}{\mathrm{d}V^3}\right|_{V_\mathrm{DC}} {V_\mathrm{p}}^3 \cos 3\omega_\mathrm{p} t + \frac{1}{192}\left.\frac{\mathrm{d}^4 C_\mathrm{s}}{\mathrm{d}V^4}\right|_{V_\mathrm{DC}} {V_\mathrm{p}}^4 \cos 4\omega_\mathrm{p} t + \cdots \quad (1)$$

Therefore, by measuring the *n*-th order harmonic ($n\omega_\mathrm{p}$), *n*-th order capacitance response $\mathrm{d}^n C_\mathrm{s}/\mathrm{d}V^n$ is measured. The amplitude and phase of *n*-th harmonic extracted by lock-in amplifiers represent the magnitude and sign of *n*-th derivative of C-V characteristics. The super-higher-order SNDM acquires not only $1\omega_\mathrm{p}$ image, but also $2\omega_\mathrm{p}$, $3\omega_\mathrm{p}$, and $4\omega_\mathrm{p}$ images.

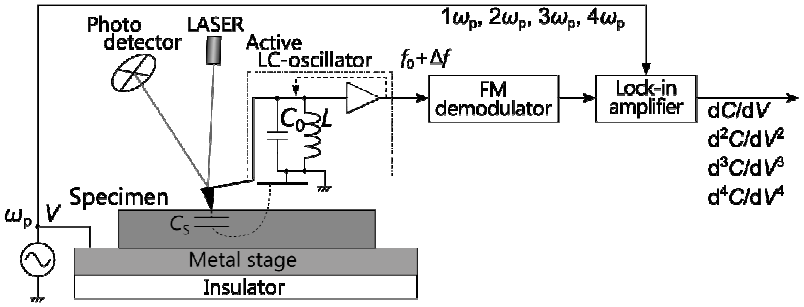

Figure 1. Schematic diagram of contact-mode AFM based SNDM.

3. Experimental result and discussion

In order to demonstrate the usefulness of the super-higher-order method, we measured the cross-section of an n-channel MOSFET whose channel length is 80 nm. We used a commercial AFM (SPA300HV, Seiko Instrument Inc.) for maintaining the tip-sample contacting force and simultaneous acquisition of topography. The cantilever was a metal (Pt-Ir) coated conductive cantilever tip with the nominal tip radius of 25 nm and spring constant of 2.8 N/m (EFM, nanosensors). In order to obtain

super-higher-order harmonics, we developed a high sensitive SNDM probe, whose oscillating frequency is about 4 GHz. For demodulating the output of the probe and for extracting amplitude and phase of each harmonic, we used a commercial modulation analyser (MS616B, Anritsu) and digital lock-in amplifier (LI5640, NF corp.). The measurement was done in air, and other conditions were as follows: $V_{\mathrm{p}} = 3\,\mathrm{V}, V_{\mathrm{DC}} = -1.5\,\mathrm{V}, f_{\mathrm{p}} = \omega_{\mathrm{p}} / 2\pi = 23\,\mathrm{kHz}$.

Figures 2 (a)–(d) show the acquired SNDM images of 1–4 ω_{p} [14]. These four SNDM images (Figs. 2 (a)–(d)) reveal the MOSFET structure; gate (G) and source/drain (S/D). The S/D region is visualized as dark in Fig. 2 (a) where the $\mathrm{d}C_{\mathrm{s}} / \mathrm{d}V$ is negative since the S/D region is n-type. We can see that images of $\mathrm{d}^3C_{\mathrm{s}} / \mathrm{d}V^3$ and $\mathrm{d}^4C_{\mathrm{s}} / \mathrm{d}V^4$ (super-higher-order ones) visualize the MOSFET in more detail than ones of $\mathrm{d}C_{\mathrm{s}} / \mathrm{d}V$ and $\mathrm{d}^2C_{\mathrm{s}} / \mathrm{d}V^2$ [14].

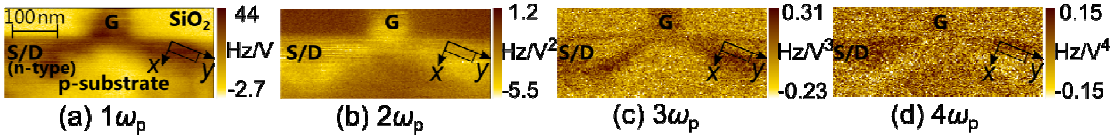

Figure 2. Acquired images of $\mathrm{d}^nC / \mathrm{d}V^n, n = 1, 2, 3, 4$. Reprinted with permission from Appl. Phys. Lett. **101**, 213112 (2012). Copyright 2012 American Institute of Physics

In order to discuss the acquired images in more detail, we extracted lineprofiles from the marked areas in four SNDM images along the *x*-direction. Since the signal-to-noise ratio was not sufficient, the lineprofiles were averaged in the *y*-direction. The averaged lineprofiles are shown in Figs. 3 (a)–(d), which correspond to positional dependencies of $\mathrm{d}C_{\mathrm{s}} / \mathrm{d}V$ – $\mathrm{d}^4C_{\mathrm{s}} / \mathrm{d}V^4$ signals. The $\mathrm{d}C_{\mathrm{s}} / \mathrm{d}V$ signal kept a constant negative value and the $\mathrm{d}^2C_{\mathrm{s}} / \mathrm{d}V^2$ signal kept an almost constant positive value. In contrast, the super-higher-order signals ($\mathrm{d}^3C_{\mathrm{s}} / \mathrm{d}V^3$ and $\mathrm{d}^4C_{\mathrm{s}} / \mathrm{d}V^4$) had strong dependence on position along the *x*-axis. Along the *x*-axis, the $\mathrm{d}^3C_{\mathrm{s}} / \mathrm{d}V^3$ signal varied from nearly 0 to a negative value and the $\mathrm{d}^4C_{\mathrm{s}} / \mathrm{d}V^4$ signal varied from a negative value to 0.

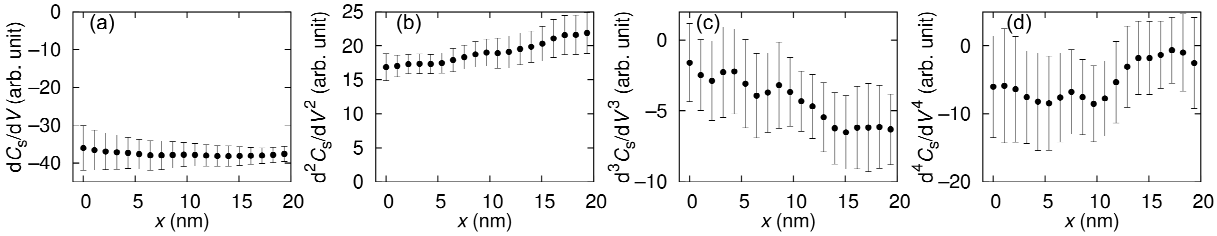

Figure 3. The averaged lineprofiles extracted from areas marked in Figs. 2 (b)–(e). Each graph represents the positional dependence along the *x*-axis of $\mathrm{d}^nC_{\mathrm{s}} / \mathrm{d}V^n, n = 1, 2, 3, 4$.

To explain these signal variations, we considered how the $\mathrm{d}^nC_{\mathrm{s}} / \mathrm{d}V^n$ signals behave depending on the small change of carrier density. Table 1 (a)–(d) shows schematic graphs illustrating the relationship between $\mathrm{d}^nC_{\mathrm{s}} / \mathrm{d}V^n$ and stage voltage V in two cases: low carrier density and high density. The illustrated graphs in these two carrier density conditions are very close since the absolute difference in density is quite small. The graphs in the low carrier density case are a little shrunk along *V*-axis compared to graphs in the high carrier density case. When the carrier density slightly decreases, the signals from $\mathrm{d}C_{\mathrm{s}} / \mathrm{d}V$ to $\mathrm{d}^4C_{\mathrm{s}} / \mathrm{d}V^4$ at $V = V_{\mathrm{DC}}$ vary in the following manner. The $\mathrm{d}^3C_{\mathrm{s}} / \mathrm{d}V^3$ varies from ~0 to negative and $\mathrm{d}^4C_{\mathrm{s}} / \mathrm{d}V^4$ varies from negative to ~0. On the other hand, variation of

dC_s/dV and d^2C_s/dV^2 are not clear. Comparing the schematic behaviour of each derivative and the behaviour with acquired data shown in Figs. 3 (a)–(d), we can understand that the carrier density decreased along the *x*-axis. This result indicates that the super-higher-order method has the potential for measuring small spatial deviations of carrier density that cannot be clarified by conventional local dC_s/dV measurement.

Table 1: Schematic graphs illustrating the relationship between $d^nC_s/dV^n (n = 1, 2, 3, 4)$ and stage voltage *V* in the n-type region corresponding to (A) high carrier density and (B) low carrier density.

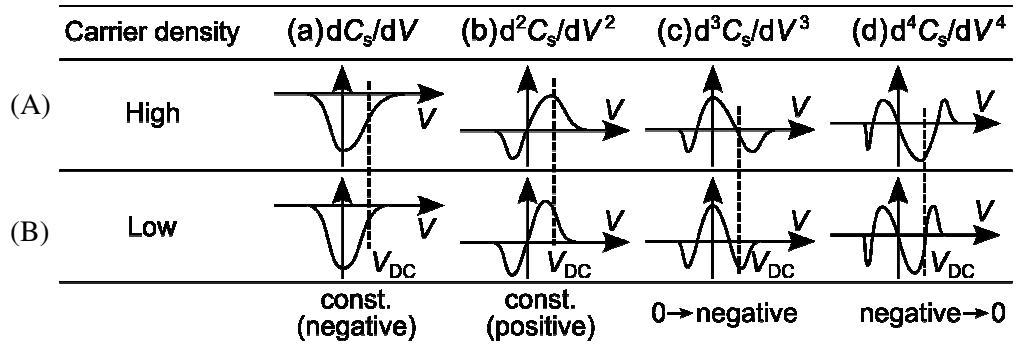

4. Conclusion

We demonstrated that the super-higher-order method can reveal small variations of carrier density that cannot be detected by conventional local dC_s/dV measurement through the cross-sectional imaging of a MOSFET. This method will be useful for precise carrier density analysis in semiconductor devices.

Acknowledgement

We would like to acknowledge Masao Uno of Murata Manufacturing Co. Ltd. and Toshihiko Iwai of Research Institute of Electric Communication, Tohoku University, for supporting the development of the high-sensitive SNDM probe. This work is partly supported by a Grant-in-Aid Scientific Research S (23226008) from the Japan Society for the Promotion of Science.

References

[1] Schwierz F *et al* 2010 *Nanometer CMOS* (Pan Stanford Publishing Pte. Ltd., Singapore)
[2] *International Technology Roadmap for Semiconductors*, 2011 edition, Process Integration, Devices, and Structures (Semiconductor Industry Association, 2011)
[3] Shibata N *et al* 2012 *International Solid State Circuit Conference* 25.1
[4] Migita S, Morita Y, Masahara M and Ota H 2012 *International Electron Devices Meeting* 8.6
[5] Hoeneisen B and Mead C A 1972 *Solid-State Electron.* **15** 819
[6] Shafai C, Thomson J D and SimardNormandin M 1994 *J. Vac. Sci. Technol. B* **12** 378
[7] Williams C C *et al* 1989 *Appl. Phys. Lett.* **55** 1662
[8] Cho Y, Kirihara A, and Saeki T 1996 *Rev. Sci. Instrum.* **67** 2297
[9] Masahara M et al 2004 *Appl. Phys. Lett.* **85** 4139
[10] Ishikawa K, Honda K and Cho Y *et al* 2006 *Nanotechnology* **17** S1
[11] Honda K, Hashimoto S and Cho Y 2005 *Nanotechnology* **16** S90
[12] Cho Y 2011 *J. Mater. Res.* **26** 2007
[13] Cho Y and Ohara K 2001 *Appl. Phys. Lett.* **79** 3842
[14] Chinone N, Yamasue K, Honda K and Cho Y 2012 *Appl. Phys. Lett.* **101** 213112